Single-molecule binding assay using nanopores and dimeric NP conjugates

Ren Ren[1‡], Maozhong Sun[2‡], Pratibha Goel[1], Shenglin Cai[1], Nicholas A. Kotov[3,4], Hua Kuang[2], Chuanlai Xu[2], Aleksandar P. Ivanov[1*], Joshua B. Edel[1*]*

‡These authors contributed equally to this work.

Dr. Ren Ren, Dr. Pratibha Goel, Dr. Shenglin Cai, Dr. Aleksandar Ivanov, Prof. Joshua B. Edel

Address: Department of Chemistry, Molecular Science Research Hub, Imperial College London, White City Campus, 82 Wood Lane, London, W12 0BZ, United Kingdom

Prof. Maozhong Sun, Prof. Hua Kuang, Prof. Chuanlai Xu

Address: Key Lab of Synthetic and Biological Colloids, Ministry of Education, State Key Lab of Food Science and Technology, International Joint Research Laboratory for Biointerface and Biodetection, School of Food Science and Technology, Jiangnan University, Wuxi, Jiangsu, 214122, P. R. China

Prof. Nicholas A. Kotov

Address: Department of Chemical Engineering, University of Michigan, Ann Arbor, MI 48109, USA

Department of Materials Science and Engineering, University of Michigan, Ann Arbor, MI 48109, USA

Email: xcl@jiangnan.edu.cn, alex.ivanov@imperial.ac.uk, joshua.edel@imperial.ac.uk

Keywords: Nanopore sensing, diagnostics, screening, molecular probes, self-assembly, single-molecule detection

Abstract: The ability to measure biomarkers, both specifically and selectively at the single-molecule level in biological fluids, has the potential to transform the diagnosis, monitoring, and therapeutic intervention of diseases. The use of nanopores has been gaining prominence in this area, not only for sequencing but more recently in screening applications. The selectivity of nanopore sensing can be substantially improved with the use of tags, but substantial challenges remain, especially when trying

to differentiate between bound from unbound targets. Here we design highly sensitive and selective molecular probes made from NPs designed specifically for nanopores that self-assemble and dimerise upon binding to a biological target. We show that both single and paired NPs can be successfully resolved while improving the time and sensitivity of the biomarker detection. Nanopore sensing with NP conjugates can be used for applications such as antigen/antibody detection for sepsis screening and miRNA sequence analysis relevant to prostate cancer. We believe that such technology opens the doors to developing a highly sensitive and selective strategy for diagnosis and screening of diseases without the need for sample processing or amplification while requiring minimal sample volume.

1. Introduction

Early-stage screening and rapid diagnosis are essential steps in improving the effectiveness of therapeutic intervention. To this end, there has been a considerable drive to developing ultra-sensitive biomarker detection strategies with single-molecule sensitivity. With such tools, it becomes possible to screen for targets with very low abundance within complex media such as serum, urine, and cerebral spinal fluid. One approach that has been gaining attention is nanopore sensing. Although DNA sequencing and DNA detection have been the major driving force[1], more recently, there has been progress in using nanopores for the detection and sensing of protein[2], nanoparticles (NPs)[3], neurotransmitters[4] and other biomolecules.[1f, 5] The popularity is in large part due to the simplicity of the approach. When nanopores reach critical diameter in the range of single nanometres, molecules are translocated one at a time through a nanometre-sized pore using an applied electric field across an insulating membrane.[1a, 1b, 6] [7] Individual analytes are detected by observing changes in the transients of the ionic current. The magnitude, dwell time, and frequency of these transients reveal information such as size[2b, 8], charge[9], shape[8, 10], dipole[11], concentration[12], and in the case of nucleic acids, even the sequence[13]. However, the detection of proteins adds significant complexity both in terms of sensitivity and selectivity. Proteins, unlike DNA, have a heterogeneous charge and typically translocate faster than can be detected, and when they do, they often exhibit a lower signal-to-noise. Besides, detection of biomolecules with nanopores is generally sensitive to the volume, and the surface charge of the analytes and improvements in the method are needed to accurately distinguish between molecules with very similar size and charge

composition. To date, much effort was invested to remedy these issues, which include functionalisation of the nanopore lumen with binding moieties[14], incorporation of field-effect-transistors[15], and use of high bandwidth instruments[16]. One of the most promising strategies is based on the use of molecular carriers such as NPs [17] and DNA[12b, 18].

These carriers can be designed to bind to a target biomarker selectively (usually using a grafted aptamers or antibodies) and subsequently translocate through the nanopore for detection. When a biomarker bound to the molecular carrier passes through the nanopore, a multilevel current signal is often observed, with the first level originating from the carrier and the secondary level caused by the biomarker. A number of groups, including our own, have already utilised DNA based molecular carriers to detect specific biomolecules with high sensitivity.[12b, 18b, 19] However, it is difficult to distinguish between the secondary signal arising due to a partially folded DNA carrier and that of the target analyte. In addition, when the size of the target is small, the secondary level can be masked by background noise. To address these limitations, we have designed a series of molecular probes based around the use of gold NPs, which have shown that it is possible to design dimeric NPs linked by either dsDNA[20] or antigen/antibodies[21].

Our strategy relies on differentiating between monomeric and dimeric NP probes that are sensitive to the presence of proteins or miRNA, **Figure 1**. The target biomarker triggers the self-assembly and dimerisation of the monomeric NPs. Distinguishing monomers and dimers is inherently simple as only a single peak in the translocation signal would be observed for a monomeric NP. In contrast, a dimeric NP produces a doublet and hence confirms the presence of the target biomarker. A unique advantage of this strategy is that it becomes possible to sense relatively small molecules, not easily detected with solid-state nanopores, as the signal originates from the NP rather than the target analyte. We validated this strategy with two classes of molecular probes: 1) antigen bound NPs for detection of procalcitonin (PCT) essential for the diagnosis of sepsis[22] (**Figure 1b**); 2) nucleic acid

bound NPs for the detection of short miRNA sequences which are upregulated in patients with active prostate cancer[23] (**Figure 1c**). By measuring the ratio between the detected monomers and dimers, we show that it is possible to determine the concentration of the biomarker with high sensitivity and selectivity at the single-molecule level.

Importantly both strategies are fully adaptable to studying alternative targets by functionalising the NP with almost any desired antibody or nucleic acid sequence.

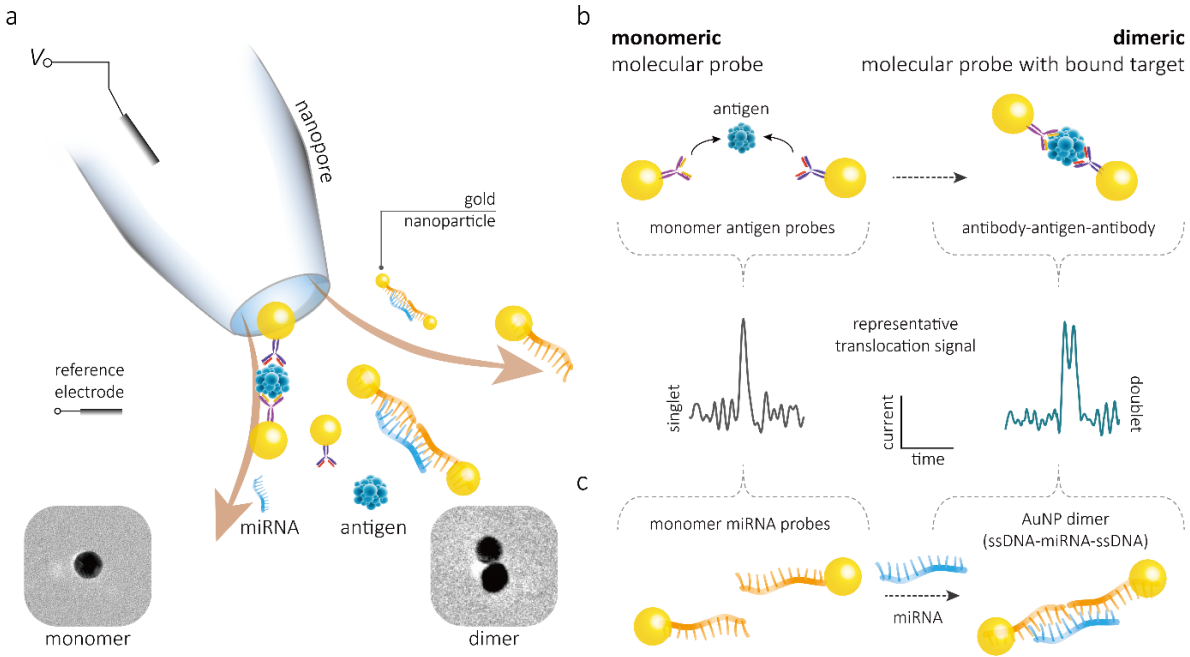

Figure 1. (**a**) Schematic of the platform along with cartoon representation of monomeric and dimeric NPs being transported though the nanopore. The translocation signal can be used to differentiate between AuNP monomers and dimers and as a result selectively determine the concentration of target analytes. (**b**) Monomeric NPs (17-20 nm) modified with antibodies can be used to initiate self-assembly and dimerisation in the presence of an antigen. This can be quantified by measuring the number of doublets versus singlets in the translocation signal. Nanopore diameter: (26 ± 4 nm) (**c**) A similar strategy can be used for the selective detection of miRNA. Two populations of NPs can be modified to contain half of the complementary miRNA sequence. In the presence of miRNA the monomeric NPs will self-assemble and dimerise. By quantifying the fraction dimerised it becomes possible to determine the analyte concentration.

2. Result and discussion

2.1. Qualification of AuNP monomers, dimers, and trimers

To validate the screening ability of the AuNP conjugates, we first confirmed that the experimental set-up had sufficient resolution to differentiate between monomeric and dimeric NPs. Initially, the spacing between NPs was controlled by using double-stranded DNA spacers, **Figure 2**. AuNP symmetrical dimers (**Figure 2b**) were fabricated by self-assembly of two 17 ± 3 nm AuNP monomers, each consisting of 1.5 single thiolated DNA strand (10 base linker and 15 bases complementary sequence) on average. Upon hybridisation, the NPs were separated by 35 base dsDNA spacer. To further assess the spatial resolution, asymmetric dimers consisting of 10 nm and 20 nm AuNP monomers were also used, **Figure 2c**. Finally, trimers were also synthesised and assembled by controlling the NP monomer ratio, **Figure 2d**. Detailed synthesis protocols and schematics of the molecular carrier designs used can be found in **Supplementary Note 1** and **Figure S1**, respectively. The geometry and size of the nanostructures were confirmed by transmission electron microscopy (TEM), **Figure 2a-d**. All NP conjugates were dispersed after synthesis in a 50 mM KCl, 10 mM Tris-EDTA buffer. The stability was confirmed by monitoring the UV-Vis spectra after 24 hours and prior to nanopore experiments. The ionic strength of the solutions was optimised to be close to physiological conditions while minimising NP aggregation and maximising the signal-to-noise of the translocation signal.

Nanopore experiments were performed with nanopipettes fabricated by laser-assisted pulling using single-barreled quartz capillaries. [24] The nanopores around 25 nm were pulled to be on average slightly larger than the diameter of the NPs, as measured by scanning electron microscopy (SEM), **Figure S2**. These dimensions closely matched the diameters (26 ± 4 nm) estimated from nanopore conductance measurements[25], 15.3 ± 2.4 nS in 100 mM KCl (n =

18), **Figure S3**. From SEM imaging, the taper angle of the nanopipette tip was measured to be 16.9 ± 1.1° over the first 100 nm (n=18), **Figure S4**, which allowed us to estimate the effective sensing length to be between 25-50 nm, calculated based on a 75-80% resistance drop at the nanopore (**Supplementary Note 2**, **Figure S5-S6**). The analyte was filled inside the nanopipette, where an AgCl patch electrode was placed. A ground/reference AgCl electrode was placed in the bath, outside the pipette. By applying a negative potential, it was possible to transport the AuNPs from inside (cis) to outside (trans) of the nanopipette. Chronoamperometric traces (I-t) were recorded at clamped voltage using a high bandwidth amplifier (Chimera Instruments, VC100) with a 1 MHz sampling rate and a 100 kHz low-pass digital filter.

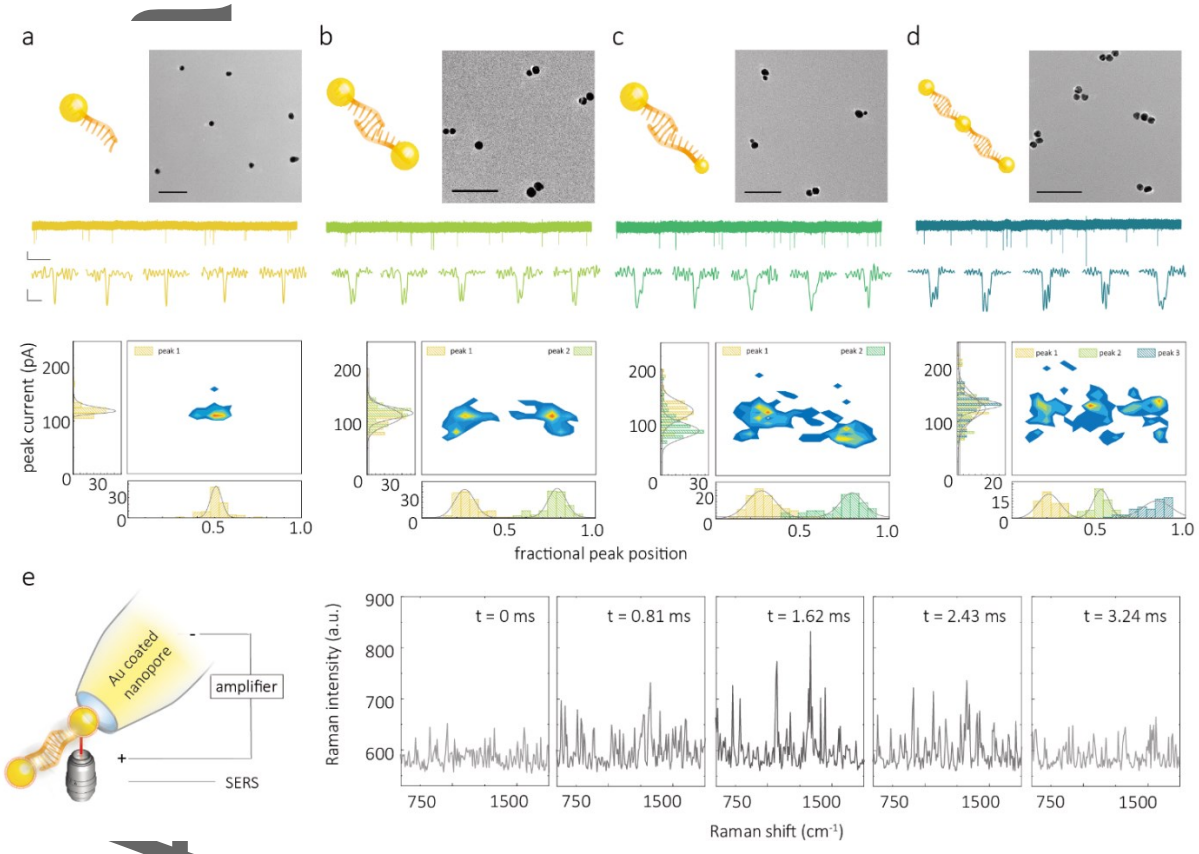

Figure 2. TEM images (Scale bar, 100 nm), and current-time trace for (**a**) AuNP monomers (**b**) AuNPs symmetrical dimers (**c**) AuNPs asymmetrical dimers and (**d**) AuNPs trimers. The scale bar for the current-time trace is 50 pA (vertical) and 5s (horizontal) respectively.

Typical individual translocation events are also shown and have a scale bar of 50 pA and 20 µs. All the translocation experiments were performed in 50 mM KCl, 10 mM Tris-EDTA and at a potential of -600 mV. Surface density plots of peak current versus fractional peak position are also shown and clearly shows that the translocation signal can differentiate between monomers, dimers, and even trimers. (**e**) Single molecule SERS was also used to confirm NP dimerisation along with translocation through the nanopipette. The NPs were coated with 4-Aminothiophenol and the nanopipette was coated in gold to maximise SERS enhancement. The spectra were recorded using a dwell time of 810 µs and translocation experiments were performed at -800 mV. An example of a sequence of SERS spectra for a single 4 ms translocation event is shown.

At low salt concentration, small, charged conical nanopores exhibit ion-perm selectivity and significant ion concentration polarisation.[26] This phenomenon leads to transient current increase when species with high surface charge density such as DNA or AuNP are translocated through the nanopore. In our case, current transients (net negative current increase at negative voltage) corresponding to the translocation of single NPs were recorded based on their dwell time and current amplitude increase. A comparison of the translocation characteristics for the different conjugates, including representative traces, individual translocation events, and scatter plots and histograms of dwell time and peak current, is shown in **Figure 2**. The nanopore translocation of the simplest constructs, AuNP monomers, resulted in relatively quick events with a mean dwell time of 8 ± 1 µs at an applied potential of -600 mV), and a current distribution with a single peak (singlet), **Figure 2a** and **Figure S7**. The distribution of the dwell times was normalised, with 0 being defined as the translocation onset and 1 being defined as the end of the translocation and plotted as a fractional position.[12b] This is needed to take into account the difference in dwell times from translocation to translocation so that the fractional position of the current peak maxima or the translocation time between two monomers in a doublet could be compared. Symmetric and asymmetric dimers with a 35 base DNA spacer showed fractional position plots with clear doublet distribution, **Figures 2b-c**, and comprised of dwell times just over twice in duration

when compared to the monomer (**Figure S7**). The distribution doublets observed in the current amplitude were consistent with the translocation of the dimers in a linear conformation, i.e., the first peak appears as a net current amplitude increase due to the translocation of the AuNP. A decrease in current follows as a result of the transport of the linker through the nanopore. Finally, a second peak appears as the second AuNP in the dimer translocates through the nanopore. Notably, one could distinguish between the doublet peaks with high temporal resolution even though the spacing was only 28 - 51 nm in length. Further studies on the voltage dependence and comparison between AuNP symmetrical dimers with different linker lengths (35 bases and 115 bases) are shown in **Figure S8** and **Figure S9**, respectively.

For asymmetric dimers, **Figure 2c**, the size of the individual NPs was reflected in the shape and the current amplitude for each peak in the doublet. As an example, peak currents of 155.5 ± 21.6 pA and 81.8 ± 13.5 pA corresponded to the translocation of the 20 nm and 10 nm AuNP in the dimers. Interestingly, 92 ± 4 % of all translocation events of asymmetric dimers showed a preferential orientation with the larger NP being transported first, which was attributed to the larger NPs carrying higher surface charge. Although not the focus of the present manuscript, we also investigated the possibility of translocating and detecting NP trimers, **Figure 2d**. Trimers could be detected and resolved, as observed with a typical triplet signature in the ionic current and three distinct populations in the fractional peak position. Trimers, on average, took 33 ± 5 μs to translocate through the nanopore, which is 3.94-fold and 1.57-fold longer than the respective dwell times for monomers and dimers. This is in good agreement due to a change in spatial length for which the trimer is 4.23-fold and 1.61-fold longer than the monomer and dimer, respectively. Measurements containing a mixture of

monomer, dimer, and trimers were also performed, and clear single, double and triple events could be observed (**Figure S10)**.

To further characterise the translocations of these metallic NPs, single-particle surface-enhanced Raman scattering (SERS)[27] was also performed on a modified nanopore coated with 10nm thick gold, **Figure S11-12**, **Supplementary Note 3**. Due to the coupling and proximity between the dimers and the surface of the nanopore, a significant enhancement in the Raman signal could be obtained.[28] To achieve single-particle SERS, somewhat larger 35 nm, AuNP symmetrical dimers were used due to the higher scattering cross-section. The AuNPs were functionalised with 4-Aminothiophenol (ATP) dye, **Figure 2e**. The dimer was further stabilised with polyethylene glycol (PEG) to ensure the particles do not aggregate at the 100 mM salt concentrations required to perform the translocations. A typical SERS spectrum of the NPs in bulk solution is shown and consists of expected peaks at 1138, 1387, and 1571 cm^{-1}, **Figure S13**. This is comparable to the data obtained for single-particle SERS, seen from the transients, **Figure 2e**. In this example, the dwell times recorded optically were 3.24 ± 0.81 ms, which is longer than the corresponding electrical events (0.79 ± 0.29 ms), **Figure S14**. This is due to the nanopore sensing region being much smaller than the diffraction-limited laser spot size (ca. 1 μm). As a negative control, Raman spectra, which show no Raman signal, were also acquired when a reverse potential was applied, **Figure S15**. We envisage that this method can also be used to perform molecular assays and complement electrical detection shown in this manuscript and simultaneous electro-optical sensing, as previously published by our group.[12a, 29] In the future, combined nanopore sensing with SERS single-molecule detection can likely provide an additional modality that is particularly useful in the context of using large nanopore arrays.

2.2. Molecular probes for single-molecule detection of miRNA

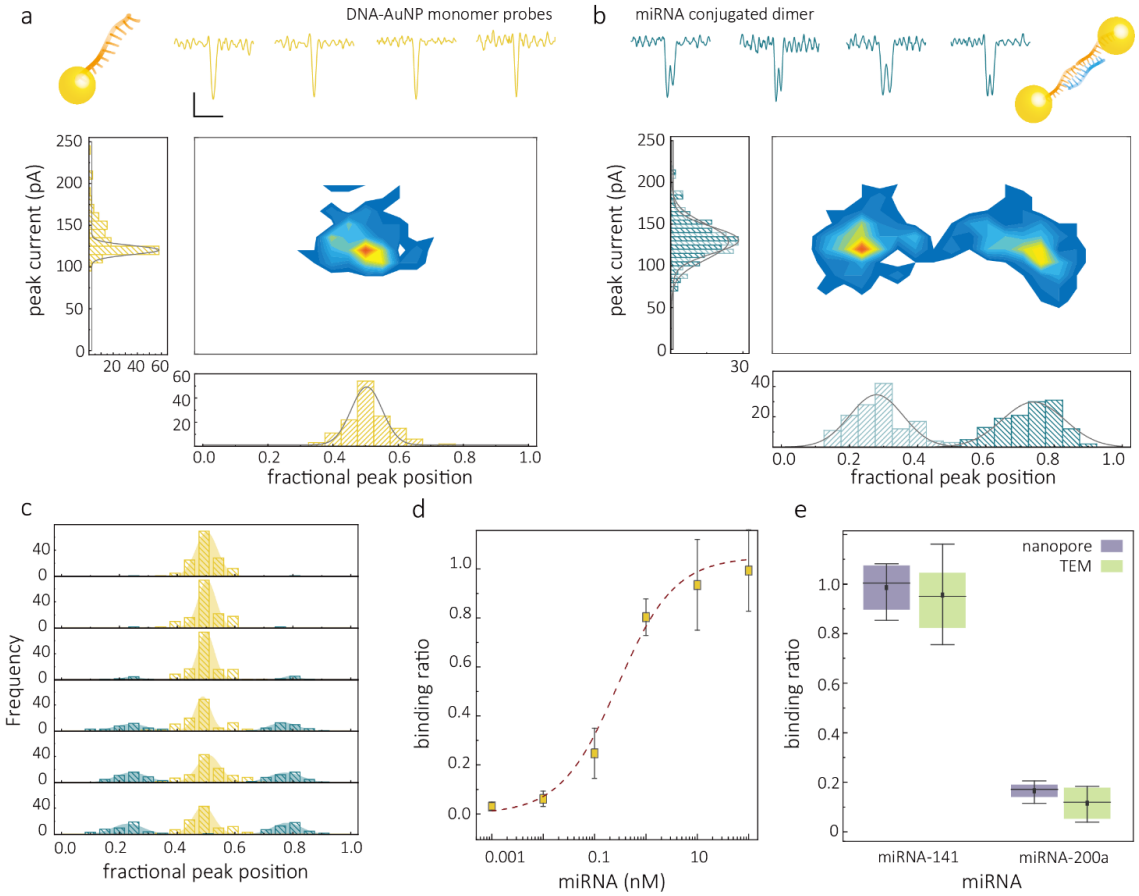

Figure 3. Nanopore sensing of mRNA-141. (**a**) AuNP monomer miRNA-141 molecular probes. Representative individual translocation events are shown (Scale bar: vertical 50 pA, horizontal 20 μs) along with associated statistics. (**b**) Conjugated dimers with miRNA141linked between 2 NP monomers. All the translocation experiments were performed in 50 mM KCl, 10 mM Tris-EDTA and at a potential of -600 mV. (**c**) The normalised peak position of the monomer probe and conjugated dimer with different concentration of mRNA-141 (From top to bottom, 0 nM, 10 pM, 100 pM, 1 nM, 10 nM and 100 nM). (**d**) the binding curve of 2 nM AuNP monomer miRNA-141 probes incubating with the target miRNA ranging from 0 to 100 nM. (**e**) The comparison of the detection of miRNA-141 and miRNA-200a using AuNP monomer miRNA-141 probes. Error bars represent the standard deviation of three independent experimental repeats.

miRNA are a class of short non-coding RNAs that function in RNA silencing and post-transcriptional gene regulation. Besides their participation in regulating normal physiological activities, specific miRNA types could act as oncogenes, tumour suppressors, or metastasis regulators, which are critical biomarkers for cancer. Conventional methods include Northern blotting, in situ hybridisation, RT-qPCR, or microarrays. However, these methods require

sample preparation or processing. Also, each technique has specific limitations such as low throughput and low sensitivity (for northern blotting), semi-quantitative (for in situ hybridisation), time-consuming, specific reaction conditions (for RT-qPCR), high cost and relative low accuracy (for microarrays). Recent advances in nanopore technology offer the promise of addressing some of these drawbacks for detecting miRNA with high sensitivity and selectivity.[30] However, the signal of these short fragments (typically 18-23 bases) is hard to detect directly with solid-state nanopores due to the high-speed translocation and low signal-to-noise ratio, **Figure S16**. Here, we use AuNP dimer self-assembly to amplify this translocation signal, leading to very efficient miRNA detection at the single-molecule level.

In this study, we use AuNP molecular probes for the detection of miRNA-141. miRNA-141 is commonly dysregulated in malignant tumours such as those associated with prostate cancer and plays essential roles in tumor development and progression, becoming a powerful potential biomarker of prostate cancer.[31] Prostate cancer is the second most common cancer in men worldwide; however, disease outcome is difficult to predict in large part due to the lack of efficient diagnostic strategies. As such, miRNA-141 has the potential to become a useful biomarker.

The molecular probes consisted of two populations of ssDNA functionalised to AuNP monomers. Each of them was modified by an 11 base recognition chain, which can hybridise with half of the 22-base-long miRNA-141, **Figure S17**. With the addition of the target, the monomer probes self-assemble to form dimers and produce doublet signatures, **Figure 3a-c**. A binding assay was performed within the miRNA concentration range of 1 pM to 100 nM. As previously shown for PCT, the number of dimers, hence doublets, increases with concentration **Figure 3d-e**. Dimer formation is validated and compared with TEM, **Figure S18**, providing visual evidence of dimer formation due to the presence of miRNA-141.

Typically, the concentration of miRNA-141 is between fM and pM in unprocessed prostate cancer patient samples and between pM to nM in extracted miRNA samples.

The specificity of the molecular probes was verified by detecting miRNA-200a, which is also in the miR-200 family and share seed sequences differing in only two nucleotides when compared with miRNA-141, **Figure S19**. The full recognition of miRNA-141 gives a significant binding result, whereas the control experiment, which is detecting the miRNA-200a, leads to a low value of the binding ratio, **Figure 3e**. The result is further confirmed by TEM, **Figure 3e**, **Figure S20**. Such high selective capability probably benefits from the dimerisation mechanism. For example, for miRNA-141, the monomer probes can be linked to the dimer because the ssDNA is fully matching the target. In contrast, for the miRNA-200a, the two mismatch points happened on the same ssDNA of one monomer probe, leading to a very low binding affinity, which causes unsuccessful dimerisation. This result shows that the AuNP monomer probe can detect the target with high specificity.

2.3. Molecular probes for single-molecule detection of PCT

As mentioned earlier, the detection of relatively small molecules (some small proteins, peptides, etc.) selectively using nanopores can be challenging. Molecular carriers can be used in part to tackle this issue. However, the smaller the target, the progressively harder it gets to detect the difference in signal originating from the molecular carrier and peak associated with the analyte, **Figure S22**. Building on our previous work[21], a universal strategy for sensing small antigen molecules has been developed. Here we used a mixture of AuNPs with half the population being modified with an antibody (mAb1) and the other half being modified with another antibody (mAb2). In the presence of the antigen, the AuNPs self-assemble and dimerise upon binding to the two antibodies. The presence and concentration or no presence

of the antigen can be confirmed by comparing the number of dimers (doublet peaks) versus monomers (singlet peaks), **Figure 4a-b**.

In this example, we synthesise AuNP modified with antigen probes for the detection of PCT(M.W. 14.5 kDa; pI of 6.5), which is a peptide precursor of the hormone calcitonin. Measuring the PCT level in patients has become an important indicator of identifying bacterial infections and guiding antibiotic therapy.[32] It is, therefore, essential to detect PCT at trace levels below 10 ng/ml. A comparison between the translocation of 2 nM AuNP monomers (50% are functionalised by PCT mAb1, and 50% are functionalised by mAb2) and the assembled dimer complex after adding 0.29 μg/ml (≈ 20 nM) PCT is shown in **Figure 4a-b**. Without the presence of PCT, only singlets were observed during the translocation of 2 nM AuNP monomers with 50 mM KCl, pH 8. Upon addition of 0.29 μg/ml PCT, approximately 15% of the singlet peaks become doublets. The double peak signature results from the translocating of two AuNPs linked by the mAb-PCT-sAb sandwich linker (PI of mAb1, mAb2 is 6.6-7.2). As a negative control, no doublets were observed when PCT was replaced by other antigens such as insulin, **Figure S24**.

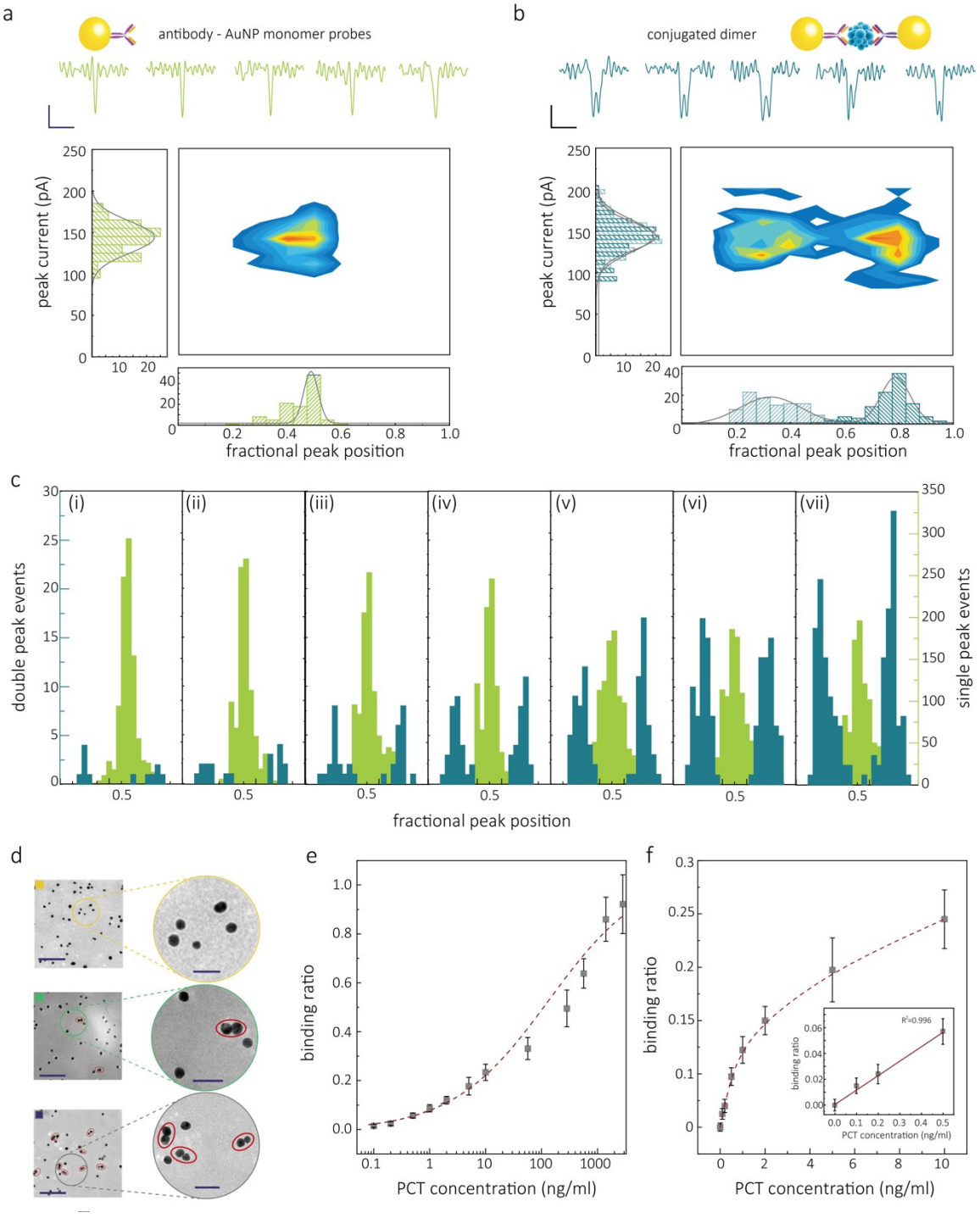

Figure 4. Nanopore sensing of PCT. (**a**) AuNP monomeric molecular probes consisting of a single antibody. Individual translocation events are shown (Scale bar: vertical 50 pA, horizontal 20 µs) along with associated statistics. (**b**) conjugated dimers linked by an antibody-antigen-antibody sandwich. All the translocation experiments were performed in 50 mM KCl, 10 mM Tris-EDTA and at a potential of -600 mV. (**c**) Normalised peak position of the monomer probe and conjugated dimer at varying PCT concentration (i) 0.1 ng/ml, (ii) 0.2 ng/ml, (iii) 0.5 ng/ml, (iv) 1.0 ng/ml, (v) 2.0 ng/ml, (vi) 5.0 ng/ml, (vii) 10.0 ng/ml. (**d**) TEM images are used to confirm successful binding (Scale bar: 200 nm, enlarged, 50 nm), from top

to bottom, 0 ng/ml, 1.0 ng/ml, 2.9 μg/ml PCT, respectively. (**e**) the binding curve of 2 nM AuNP monomer PCT probes incubating with PCT ranging from 0 to 2.9 μg/ml. (**f**) Same binding curve as in e, highlighting the clinically relevant range. A linear increase in the binding ratio is observed at low concentrations, as shown in the inset. Error bars represent the standard deviation of three independent experimental repeats.

To validate that this sandwich immunoassay can be used at clinically relevant concentrations[22b], a binding assay was performed at varying PCT concentrations. In this case, the concentration of the molecular probes was kept at 2 nM, while the concentration of PCT was varied from 0 to 10.0 ng/ml. As expected, the percentage of singlets decreased, whereas the proportion of doublets increased with the addition of PCT, **Figure 4c**. The results were further confirmed by TEM (**Figure 4d**, **Figure S25-26**), providing visual evidence of binding and NP assembly. The full binding curve with PCT ranging from 0 to 2.9 μg/ml is shown in **Figure 4e**.

Notably, at high analyte concentrations, higher-order NP aggregates were not observed, which was attributed to the effective 1:1 ratio between antibody and NP. It is important to note that all binding curves saturated at approximately 33% and was consistent with different measurement techniques. This is due to an equal probability of the solution containing two forms of the monomeric NPs bound with PCT, and dimeric NPs linked with PCT. **Figure S26**. All binding ratios were therefore normalised to the maximum value of 33%.

In bacterial infections, the concentration of PCT in plasma increases from 0.15 to more than 10 ng/ml with increasing severity of the disease. At the same time, PCT has also been used to guide antibiotic therapy; for example, if PCT levels are less than 0.1 ng/ml, antibiotic therapy is strongly discouraged; if PCT levels are greater than 1 ng/ml, antibiotic therapy is strongly encouraged[22b]. To validate that our probes have sufficient sensitivity, the limit of detection (LOD) was calculated from the linear range in **Figure 4f** and was determined to be 0.12 ng/ml. To further validate the method can be used in a complex solution, we also performed

the experiments in 1% BSA solution. The result indicates that dimers can still be discriminated at high interferent protein concentration, **Figure S27**. It should be noted that the target antigen should have two different epitopes so that the nanoparticle dimers can be formed.

3. Conclusion

We demonstrate that it is possible to design NP probes for the selective sensing of individual targets using nanopores. The assay is based on the dimerisation of individual monomeric NPs in the presence of a biomarker. We show that this strategy can be used for both protein and miRNA detection at the single-molecule level. We validated our strategy for two applications: 1) detection of procalcitonin, a biomarker of sepsis at ultra-low concentrations, and 2) highly specific detection of miRNA-141, which is a potential indicator of prostate cancer. Moreover, by correlating monomer to dimer ratio, single-molecule binding and the concentration of the analytes can be accessed.

Importantly this approach is independent of biomarker size and, in principle, can be equally efficient for the detection of both small and larger biomarkers alike. The excellent selectivity and affinity of antibody-antigen reaction and ssDNA-RNA base-pairing allow the application of these strategies to diagnostics for detecting biomarkers in trace amounts. Compared to other methods, the integration of NP assemblies with nanopore technologies leads to a much-needed combination of high-performance detection and exceptionally small sample volumes (several microlitres and below). Importantly the method is fully adaptable to studying alternative targets by functionalising the NP with almost any desired antibody or nucleic acid sequence.

4. Methods

4.1. The fabrication of nanopipettes

Single barrel quartz capillaries (o.d., 1.0 mm, i.d., 0.7 mm, Intracell) were plasma cleaned (Harrick Plasma) and pulled using a laser-based pipette puller (P-2000, Sutter Instruments). A two-line program was used (heat 800, filament 4, velocity 30, delay 170, and pull 80; heat 825, filament 3, velocity 20, delay 145, and pull 130) to produce nanopipettes with a diameter of approximately 25 nm. It should be noted that the above pulling parameters are instrument-specific, and variations will exist from puller to puller.

4.2. Assembly of AuNP based nanostructures

We used traditional methods of bioconjugation to prepare NP-based conjugates.[33] The detailed fabrication process of AuNP monomer, AuNP symmetrical dimer (35 bases or 115 bases linker), AuNP asymmetrical dimer, AuNP trimer, and 4-ATP modified dimer are shown in Supplementary Note 2.

4.3. Preparation of monomer PCT probes

The antibody for PCT (mAb) was prepared in our lab. Initially, we obtained the antibody by a eukaryotic expression system and then immunized the mice. This was followed by screening and measuring the selectivity and affinity between the antigen and antibody. AuNPs were then functionalised with mAb and bound via electrostatic interactions. 2 mL AuNPs (2 nM, 20 ± 3 nm) were centrifuged for 10 min at 8000 rpm and then resuspended in 200 μL of 10 mM phosphate bu□er (PB) solutions, which was adjusted to pH 9 with 0.1 M K2CO3. Next, 100 μL of the AuNPs were conjugated with anti-PCT mAb1 (10 μL, 100 μg/mL), and the other 100 μL AuNPs were modified with anti-PCT mAb2 (10 μL, 100 μg/mL), respectively. The AuNPs were blocked using a solution of BSA (10 μL, 500 μg/mL). Finally, the functionalised AuNPs were centrifuged for 10 min at 7500 rpm at 4 °C. After centrifugation,

the supernatant was discarded and the AuNPs were resuspended in 0.02 M Tris-HCl, 0.1% Tween-20, 0.1% PEG, 1% PVP, 5% sucrose, 4% trehalose, 2% sorbitol, 1% mannitol. 0.04% NaN3, and 0.2% BSA, 1 mL.

4.4. Translocation experiments

The buffer used in the translocation experiments consisted of 50 mM KCl and 10 mM Tris-EDTA (pH=8) unless reported otherwise. For the binding assays, 1 nM molecular probes were used and incubated with the target analytes at a different concentration for at least 2 hrs. Approximately 10 µL of the electrolyte was filled inside the nanopipettes via a Microfil needle (MF34G, World Precision Instruments, UK). Freshly made Ag/AgCl electrodes were then inserted into the nanopipette and the bath. All ion current recording was performed using a high bandwidth amplifier VC100 (Chimera Instruments). The recorded data were resampled to 1 MHz and filtered at 100 kHz. Analysis of all translocations events was performed using custom-written Matlab code, The Nanopore App. The detailed data analysis workflow is shown in **Supporting Information Section S7**, **Figure S28**.

Author Contributions

‡RR and MZS contributed equally to this work.

JBE, API, NK, and CLX designed and supervised the research. RR and MZS performed experiments and contributing equally to this work. The manuscript was written through the contribution of all authors. All authors have given approval to the final version of the manuscript.

Acknowledgement

API and JBE acknowledge support from BBSRC grant BB/R022429/1, EPSRC grant EP/P011985/1, and Analytical Chemistry Trust Fund grant 600322/05. This project has also

received funding from the European Research Council (ERC) under the European Union's Horizon 2020 research and innovation program (grant agreement No 724300 and 875525). MZS acknowledges support from the Young Elite Scientist Sponsorship Program by CAST 2019QNRC001 , 51802125 , 21977038 , BK20180605 , JUSRP22037.

Received: ((will be filled in by the editorial staff))
Revised: ((will be filled in by the editorial staff))
Published online: ((will be filled in by the editorial staff))

References

[1] a) B. N. Miles, A. P. Ivanov, K. A. Wilson, F. Dogan, D. Japrung, J. B. Edel, *Chem. Soc. Rev.* **2013**, 42, 15; b) A. Meller, L. Nivon, D. Branton, *Phys. Rev. Lett.* **2001**, 86, 3435; c) M. Wanunu, *Phys. Life. Rev.* **2012**, 9, 125; d) Y. L. Ying, J. J. Zhang, R. Gao, Y. T. Long, *Angew. Chem. Int. Ed.* **2013**, 52, 13154; e) Z. T. Zhu, X. Z. Duan, Q. Li, R. P. Wu, Y. S. Wang, B. L. Li, *J. Am. Chem. Soc.* **2020**, 142, 4481; f) O. K. Zahid, F. Wang, J. A. Ruzicka, E. W. Taylor, A. R. Hall, *Nano Lett.* **2016**, 16, 2033; g) P. Karau, V. Tabard-Cossa, *Acs Sensors* **2018**, 3, 1308.

[2] a) C. Plesa, S. W. Kowalczyk, R. Zinsmeester, A. Y. Grosberg, Y. Rabin, C. Dekker, *Nano Lett.* **2013**, 13, 658; b) W. Li, N. A. W. Bell, S. Hernandez-Ainsa, V. V. Thacker, A. M. Thackray, R. Bujdoso, U. F. Keyser, *ACS nano* **2013**, 7, 4129; c) L. J. Steinbock, S. Krishnan, R. D. Bulushev, S. Borgeaud, M. Blokesch, L. Feletti, A. Radenovic, *Nanoscale* **2014**, 6, 14380; d) Q. Li, Y. L. Ying, S. C. Liu, Y. Lin, Y. T. Long, *Acs Sensors* **2019**, 4, 1185. e) S.-C. Liu, Y.-L. Ying, W.-H. Li, Y.-J. Wan, Y.-T. Long, Chemical Science 2021, DOI: 10.1039/D0SC06106A; e) S.-M. Lu, X.-Y. Wu, M.-Y. Li, Y.-L. Ying, Y.-T. Long, View 2020, 1, e72. f) Z. L. Hu, M. Z. Huo, Y. L. Ying, Y. T. Long, Angewandte Chemie-International Edition, DOI: 10.1002/anie.202013462.

[3] a) W. J. Lan, D. A. Holden, B. Zhang, H. S. White, *Anal. Chem.* **2011**, 83, 3840; b) M. Tsutsui, S. Hongo, Y. He, M. Taniguchi, N. Gemma, T. Kawai, *ACS nano* **2012**, 6, 3499; c) M. Davenport, K. Healy, M. Pevarnik, N. Teslich, S. Cabrini, A. P. Morrison, Z. S. Siwy, S. E. Letant, *ACS nano* **2012**, 6, 8366; d) Y. X. Wang, K. Kececi, M. V. Mirkin, V. Mani, N. Sardesai, J. F. Rusling, *Chem. Sci.* **2013**, 4, 655.

[4] D. S. Koktysh, X. R. Liang, B. G. Yun, I. Pastoriza-Santos, R. L. Matts, M. Giersig, C. Serra-Rodriguez, L. M. Liz-Marzan, N. A. Kotov, *Adv. Funct. Mater.* **2002**, 12, 255.

[5] a) H. Cai, Y. Wang, Y. Yu, M. V. Mirkin, S. Bhakta, G. W. Bishop, A. A. Joshi, J. F. Rusling, *Anal. Chem.* **2015**, 87, 6403; b) E. A. Heins, Z. S. Siwy, L. A. Baker, C. R. Martin, *Nano Lett.* **2005**, 5, 1824.

[6] a) Y. L. Ying, Y. T. Long, *J. Am. Chem. Soc.* **2019**, 141, 15720; b) C. Dekker, *Nat. Nanotechnol.* **2007**, 2, 209.

[7] S. M. Lu, Y. Y. Peng, Y. L. Ying, Y. T. Long, *Anal. Chem.* **2020**, 92, 5621.

[8] X. Wang, M. D. Wilkinson, X. Lin, R. Ren, K. R. Willison, A. P. Ivanov, J. Baum, J. B. Edel, *Chem. Sci.* **2020**, DOI: 10.1039/C9SC05710B.

[9] a) H. J. Kim, U. J. Choi, H. Kim, K. Lee, K. B. Park, H. M. Kim, D. K. Kwak, S. W. Chi, J. S. Lee, K. B. Kim, *Nanoscale* **2019**, 11, 444; b) M. Firnkes, D. Pedone, J. Knezevic, M. Doblinger, U. Rant, *Nano Lett.* **2010**, 10, 2162.

[10] N. Varongchayakul, J. X. Song, A. Meller, M. W. Grinstaff, *Chem. Soc. Rev.* **2018**, 47.

[11] J. Houghtaling, C. F. Ying, O. M. Eggenberger, A. Fennouri, S. Nandivada, M. Acharjee, J. L. Li, A. R. Hall, M. Mayer, *ACS nano* **2019**, 13, 5231.

[12] a) S. L. Cai, J. Y. Y. Sze, A. P. Ivanov, J. B. Edel, *Nat. Commun.* **2019**, 10; b) J. Y. Y. Sze, A. P. Ivanov, A. E. G. Cass, J. B. Edel, *Nat. Commun.* **2017**, 8.

[13] B. M. Venkatesan, R. Bashir, *Nat. Nanotechnol.* **2011**, 6, 615.

[14] a) B. Luan, G. Stolovitzky, G. Martyna, *Nanoscale* **2012**, 4, 1068; b) U. F. Keyser, *J. R. Soc. Interface* **2011**, 8, 1369; c) R. Wei, V. Gatterdam, R. Wieneke, R. Tampe, U. Rant, *Nat. Nanotechnol.* **2012**, 7, 257.

[15] a) L. Xue, P. Cadinu, B. Paulose Nadappuram, M. Kang, Y. Ma, Y. Korchev, A. P. Ivanov, J. B. Edel, *ACS Appl. Mater. Interfaces* **2018**, 10, 38621; b) R. Ren, Y. J. Zhang, B. P. Nadappuram, B. Akpinar, D. Klenerman, A. P. Ivanov, J. B. Edel, Y. Korchev, *Nat. Commun.* **2017**, 8; c) Y. Ai, J. Liu, B. K. Zhang, S. Qian, *Anal. Chem.* **2010**, 82, 8217; d) R. Ren, X. Y. Wang, S. L. Cai, Y. J. Zhang, Y. Korchev, A. P. Ivanov, J. B. Edel, *Small Methods*, DOI: 10.1002/smtd.202000356.

[16] a) J. Larkin, R. Y. Henley, M. Muthukumar, J. K. Rosenstein, M. Wanunu, *Biophys. J* **2014**, 106, 696; b) J. K. Rosenstein, M. Wanunu, C. A. Merchant, M. Drndic, K. L. Shepard, *Nat. Methods* **2012**, 9, 487.

[17] a) X. Y. Lin, A. P. Ivanov, J. B. Edel, *Chem. Sci.* **2017**, 8, 3905; b) H. Wang, H. R. Tang, C. Yang, Y. X. Li, *Anal. Chem.* **2019**, 91, 7965; c) T. Takakura, I. Yanagi, Y. Goto, Y. Ishige, Y. Kohara, *Appl. Phys. Lett.* **2016**, 108.

[18] a) N. A. W. Bell, U. F. Keyser, *J. Am. Chem. Soc.* **2015**, 137, 2035; b) N. A. W. Bell, U. F. Keyser, *Nat. Nanotechnol.* **2016**, 11, 645.

[19] a) A. Singer, M. Wanunu, W. Morrison, H. Kuhn, M. Frank-Kamenetskii, A. Meller, *Nano Lett.* **2010**, 10, 738; b) E. Beamish, V. Tabard-Cossa, M. Godin, *Acs Sensors* **2017**, 2, 1814; c) A. Y. Y. Loh, C. H. Burgess, D. A. Tanase, G. Ferrari, M. A. McLachlan, A. E. G. Cass, T. Albrecht, *Anal. Chem.* **2018**, 90, 14063.

[20] W. Chen, A. Bian, A. Agarwal, L. Q. Liu, H. B. Shen, L. B. Wang, C. L. Xu, N. A. Kotov, *Nano Lett.* **2009**, 9, 2153.

[21] X. L. Wu, L. G. Xu, L. Q. Liu, W. Ma, H. H. Yin, H. Kuang, L. B. Wang, C. L. Xu, N. A. Kotov, *J. Am. Chem. Soc.* **2013**, 135, 18629.

[22] a) G. A. Wanner, W. Keel, U. Steckholzer, W. Beier, R. Stocker, W. Ertel, *Crit. Care Med.* **2000**, 28, 950; b) K. Reinhart, M. Bauer, N. C. Riedemann, C. S. Hartog, *Clin. Microbiol. Rev.* **2012**, 25, 609.

[23] a) J. C. Brase, M. Johannes, T. Schlomm, M. Falth, A. Haese, T. Steuber, T. Beissbarth, R. Kuner, H. Sultmann, *Int. J. Cancer* **2011**, 128, 608; b) G. A. D. Metcalf, A. Shibakawa, H.

Patel, A. Sita-Lumsden, A. Zivi, N. Rama, C. L. Bevan, S. Ladame, *Anal. Chem.* **2016**, 88, 8091.

[24] a) L. M. Ying, S. S. White, A. Bruckbauer, L. Meadows, Y. E. Korchev, D. Klenerman, *Biophys. J* **2004**, 86, 1018; b) M. Karhanek, J. T. Kemp, N. Pourmand, R. W. Davis, C. D. Webb, *Nano Lett.* **2005**, 5, 403.

[25] D. Perry, D. Momotenko, R. A. Lazenby, M. Kang, P. R. Unwin, *Anal. Chem.* **2016**, 88, 5523.

[26] K. K. Chen, N. A. W. Bell, J. L. Kong, Y. Tian, U. F. Keyser, *Biophys. J* **2017**, 112, 674.

[27] a) M. P. Cecchini, J. Hong, C. Lim, J. Choo, T. Albrecht, A. J. Demello, J. B. Edel, *Anal. Chem.* **2011**, 83, 3076; b) Y. Ma, D. Sikdar, A. Fedosyuk, L. Velleman, D. J. Klemme, S. H. Oh, A. R. J. Kucernak, A. A. Kornyshev, J. B. Edel, *ACS nano* **2020**, 14, 328.

[28] a) J. M. Nam, J. W. Oh, H. Lee, Y. D. Suh, *Acc. Chem. Res.* **2016**, 49, 2746; b) M. P. Cecchini, A. Wiener, V. A. Turek, H. Chon, S. Lee, A. P. Ivanov, D. W. McComb, J. Choo, T. Albrecht, S. A. Maier, J. B. Edel, *Nano Lett.* **2013**, 13, 4602; c) C. R. Crick, P. Albella, H. J. Kim, A. P. Ivanov, K. B. Kim, S. A. Maier, J. B. Edel, *Acs Photonics* **2017**, 4, 2835; d) K. J. Freedman, C. R. Crick, P. Albella, A. Barik, A. P. Ivanov, S. A. Maier, S.-H. Oh, J. B. Edel, *Acs Photonics* **2016**, 3, 1036.

[29] W. H. Pitchford, H. J. Kim, A. P. Ivanov, H. M. Kim, J. S. Yu, R. J. Leatherbarrow, T. Albrecht, K. B. Kim, J. B. Edel, *ACS nano* **2015**, 9, 1740.

[30] V. P. Dave, T. A. Ngo, A.-K. Pernestig, D. Tilevik, K. Kant, T. Nguyen, A. Wolff, D. D. Bang, Laboratory Investigation 2019, 99, 452.

[31] P. S. Mitchell, R. K. Parkin, E. M. Kroh, B. R. Fritz, S. K. Wyman, E. L. Pogosova-Agadjanyan, A. Peterson, J. Noteboom, K. C. O'Briant, A. Allen, D. W. Lin, N. Urban, C. W. Drescher, B. S. Knudsen, D. L. Stirewalt, R. Gentleman, R. L. Vessella, P. S. Nelson, D. B. Martin, M. Tewari, *P. Natl. Acad. Sci. USA* **2008**, 105, 10513.

[32] M. Assicot, D. Gendrel, H. Carsin, J. Raymond, J. Guilbaud, C. Bohuon, *Lancet* **1993**, 341, 515.

[33] S. P. Wang, N. Mamedova, N. A. Kotov, W. Chen, J. Studer, *Nano Lett.* **2002**, 2, 817.

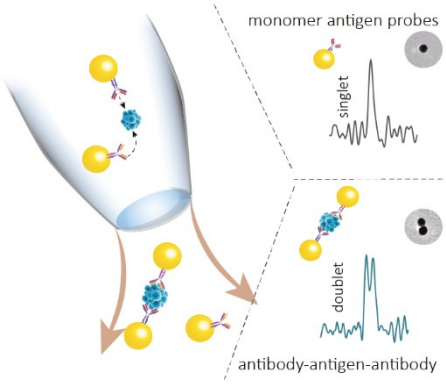

A single molecule nanopore-based sensing strategy has been developed to screen for biomarkers. In the presence of the target biomolecules, AuNPs dimerise and are detected electrically. This approach is highly sensitive and selective and can potentially be used for diagnosis and screening of diseases without the need for sample processing or amplification.